UC Davis
UC Davis Previously Published Works

Title

Spatial C 2 closed loops of prescribed arc length defined by Pythagorean-hodograph curves

Permalink

https://escholarship.org/uc/item/6g64n15k

Authors

Farouki, Rida T
Knez, Marjeta
Vitrih, Vito
et al.

Publication Date

2021-02-01

DOI

10.1016/j.amc.2020.125653

Peer reviewed

Spatial C^2 closed loops of prescribed arc length defined by Pythagorean-hodograph curves

Rida T. Farouki[a], Marjeta Knez[b,c], Vito Vitrih[d,e], Emil Žagar[*,b,c]

[a]*Mechanical and Aerospace Engineering, University of California, Davis, CA 95616, USA*
[b]*Faculty of Mathematics and Physics, University of Ljubljana, Jadranska 19, Ljubljana, Slovenia*
[c]*Institute of Mathematics, Physics and Mechanics, Jadranska 19, Ljubljana, Slovenia*
[d]*Faculty of Mathematics, Natural Sciences and Information Technologies, University of Primorska, Glagoljaška 8, Koper, Slovenia*
[e]*Andrej Marušič Institute, University of Primorska, Muzejski trg 2, Koper, Slovenia*

Abstract

We investigate the problem of constructing spatial C^2 closed loops from a single polynomial curve segment $\mathbf{r}(t)$, $t \in [0,1]$ with a prescribed arc length S and continuity of the Frenet frame and curvature at the juncture point $\mathbf{r}(1) = \mathbf{r}(0)$. Adopting canonical coordinates to fix the initial/final point and tangent, a closed–form solution for a two–parameter family of interpolants to the given data can be constructed in terms of degree 7 Pythagorean–hodograph (PH) space curves, and continuity of the torsion is also obtained when one of the parameters is set to zero. The geometrical properties of these closed–loop PH curves are elucidated, and certain symmetry properties and degenerate cases are identified. The two–parameter family of closed–loop C^2 PH curves is also used to construct certain swept surfaces and tubular surfaces, and a selection of computed examples is included to illustrate the methodology.

Key words: spatial closed–loop curves; continuity conditions; arc length; Pythagorean–hodograph curves; Euler–Rodrigues frame; tubular surfaces

2010 MSC: 51N20, 53A04, 65D17, 65H10

1. Introduction

The construction of spatial curves that form smooth closed loops is of interest in path planning problems for robotics, manufacturing, automated inspection, spatial kinematics, and related applications. Such curves are also of interest [12] in the study of *minimal surfaces*, i.e., surfaces of minimum area with prescribed boundaries, which are characterized by zero mean curvature and describe the shape of soap films with a given boundary curve.

---

[*]Corresponding author
   Email addresses: `farouki@ucdavis.edu` (Rida T. Farouki), `marjetka.knez@fmf.uni-lj.si` (Marjeta Knez), `vito.vitrih@upr.si` (Vito Vitrih), `emil.zagar@fmf.uni-lj.si` (Emil Žagar)

6 The loop closure condition $\mathbf{r}(1) = \mathbf{r}(0)$ is a minimal requirement for a closed path specified by a single parametric

7 curve segment $\mathbf{r}(t)$, $t \in [0, 1]$, but higher orders of continuity at this juncture point are typically desirable, either C^1

8 (first derivative continuity) or C^2 (first and second derivative continuity). Another desirable feature is the ability to

9 specify the total arc length S of a closed loop, to ensure that $\mathbf{r}(t)$ does not degenerate to a single point.

The parametric speed $\sigma(t)$ of a differentiable curve $\mathbf{r}(t)$ specifies the rate of change of arc length s with respect to the curve parameter t, namely

$$\sigma(t) = |\mathbf{r}'(t)| = \frac{\mathrm{d}s}{\mathrm{d}t}.$$

Among all polynomial parametric curves, the *Pythagorean–hodograph* (PH) *curves* [4] are distinguished by the property the $\sigma(t)$ is a polynomial (not the square–root of a polynomial), and consequently the cumulative arc length

$$s(t) = \int_0^t \sigma(u) \, \mathrm{d}u$$

10 is also a polynomial function. The present study shows that it is possible to construct C^2 closed loops with a

11 prescribed total arc length S using spatial PH curves of degree 7. Through adoption of a canonical coordinate

12 system, the construction can be achieved by a simple closed–form solution procedure, requiring only a few square–

13 root extractions. These C^2 closed–loop degree 7 spatial PH curves constitute a two–parameter family, with certain

14 symmetry properties achieved by appropriate choices of the free parameters.

Recall [13] that the Frenet frame on a space curve $\mathbf{r}(t)$ consists of the unit tangent $\mathbf{t}$, principal normal $\mathbf{n}$, and binormal $\mathbf{b}$, defined by

$$\mathbf{t} = \frac{\mathbf{r}'}{|\mathbf{r}'|}, \quad \mathbf{n} = \frac{\mathbf{r}' \times \mathbf{r}''}{|\mathbf{r}' \times \mathbf{r}''|} \times \mathbf{t}, \quad \mathbf{b} = \frac{\mathbf{r}' \times \mathbf{r}''}{|\mathbf{r}' \times \mathbf{r}''|}. \tag{1}$$

The variation of the Frenet frame $(\mathbf{t}, \mathbf{n}, \mathbf{b})$ along $\mathbf{r}(t)$ is specified [13] by the *Darboux vector*,

$$\mathbf{d} = \tau \, \mathbf{t} + \kappa \, \mathbf{b}, \tag{2}$$

through the relations

$$\frac{\mathrm{d}\mathbf{t}}{\mathrm{d}s} = \mathbf{d} \times \mathbf{t}, \quad \frac{\mathrm{d}\mathbf{n}}{\mathrm{d}s} = \mathbf{d} \times \mathbf{n}, \quad \frac{\mathrm{d}\mathbf{b}}{\mathrm{d}s} = \mathbf{d} \times \mathbf{b},$$

where the curvature κ and torsion τ are defined by

$$\kappa = \frac{|\mathbf{r}' \times \mathbf{r}''|}{|\mathbf{r}'|^3}, \quad \tau = \frac{(\mathbf{r}' \times \mathbf{r}'') \cdot \mathbf{r}'''}{|\mathbf{r}' \times \mathbf{r}''|^2}.$$

15 The C^2 closed–loop spatial PH curves of degree 7 constructed herein exhibit continuity of the Frenet frame and

16 curvature at the closure point $\mathbf{r}(1) = \mathbf{r}(0)$. Moreover, by an appropriate choice of the free parameters, closed loops

17 with continuity of the torsion can also be achieved.

2

The component $\tau \mathbf{t}$ of the Darboux vector (2) defines the rate of rotation of the normal $\mathbf{n}$ and binormal $\mathbf{b}$ about the tangent $\mathbf{t}$. Consequently, for a closed loop with coincident Frenet frames at $\mathbf{r}(0)$ and $\mathbf{r}(1)$, the torsion must satisfy

$$\int_0^1 \tau(t)\,\sigma(t)\,\mathrm{d}t \;=\; 2\pi k \tag{3}$$

for integer k. To preclude more than a complete rotation of $\mathbf{n}$ and $\mathbf{b}$ about $\mathbf{t}$ on traversing $\mathbf{r}(t)$, solutions with $k = 0$ are desirable, i.e., $\mathbf{r}(t)$ must have equal amounts of negative and positive torsion. It is known [1] that a smooth closed non–planar curve in $\mathbb{R}^3$ cannot have non–negative (or non–positive) torsion if it is the graph of a simple closed planar curve of positive curvature.[1]

The remainder of this paper is organized as follows. The basic system of equations that characterizes a C^1 closed loop constructed from a single PH curve segment of degree 7 is derived in Section 2, and the number of residual degrees of freedom is identified. Section 3 then investigates the extension to C^2 continuity at the juncture point $\mathbf{r}(1) = \mathbf{r}(0)$, and a closed–form solution for a two–parameter family of closed loops exhibiting continuity of position, Frenet frame, and curvature at that point is identified.

Section 4 derives the Bézier control points of the C^2 closed–loop curves, and analyzes their regularity, symmetry properties, planar instances, and the limit curve obtained as one of the parameters tends to infinity. In Section 5 we consider adapted orthonormal frames on the C^2 closed–loop PH curves, and the design of certain swept surfaces and tubular surfaces constructed from them, and the methodology is illustrated by a selection of computed examples. Finally, Section 6 summarizes the principal results of the present study, and identifies further possible avenues of investigation.

2. Spatial PH curves as closed loops

Consider the construction of spatial PH curves $\mathbf{r}(t)$, $t \in [\,0,1\,]$ that form closed C^1 loops with $\mathbf{r}(1) = \mathbf{r}(0)$, $\mathbf{r}'(1) = \mathbf{r}'(0)$, and have a prescribed total arc length S. A spatial PH curve represented as $\mathbf{r}(t) = (x(t), y(t) + \mathrm{i}\,z(t))$ may be generated [3] by integration of the Hopf map form

$$\mathbf{r}'(t) \;=\; (\,|\boldsymbol{\alpha}(t)|^2 - |\boldsymbol{\beta}(t)|^2,\, 2\,\boldsymbol{\alpha}(t)\,\overline{\boldsymbol{\beta}}(t)\,)\,, \tag{4}$$

defined in terms of two complex polynomials $\boldsymbol{\alpha}(t) = u(t) + \mathrm{i}\,v(t)$ and $\boldsymbol{\beta}(t) = q(t) + \mathrm{i}\,p(t)$. We express these polynomials in the Bernstein basis

$$b_i^m(t) \;=\; \binom{m}{i}(1-t)^{m-i}t^i\,, \quad i = 0, 1, \ldots, m,$$

---

[1] The condition (3), with $k = 0$, is also satisfied [14, 15] by curves on a sphere.

on $t \in [0, 1]$. The parametric speed of the spatial PH curve $\mathbf{r}(t)$ obtained by integrating (4) is defined by

$$\sigma(t) = |\boldsymbol{\alpha}(t)|^2 + |\boldsymbol{\beta}(t)|^2 .$$

The case of the spatial PH quintics (corresponding to $m = 2$) has already been addressed in [9]. We focus here on the degree 7 spatial PH curves ($m = 3$), constructed from cubic complex polynomials

$$\boldsymbol{\alpha}(t) = \boldsymbol{\alpha}_0 \, b_0^3(t) + \boldsymbol{\alpha}_1 \, b_1^3(t) + \boldsymbol{\alpha}_2 \, b_2^3(t) + \boldsymbol{\alpha}_3 \, b_3^3(t) ,$$
$$\boldsymbol{\beta}(t) = \boldsymbol{\beta}_0 \, b_0^3(t) + \boldsymbol{\beta}_1 \, b_1^3(t) + \boldsymbol{\beta}_2 \, b_2^3(t) + \boldsymbol{\beta}_3 \, b_3^3(t) . \tag{5}$$

To simplify the analysis we consider *canonical form* curves with $\mathbf{r}(1) = \mathbf{r}(0) = \mathbf{0}$, $\mathbf{r}'(1) = \mathbf{r}'(0) = w^2 \, \mathbf{i}$ with $w > 0$, and $S = 1$ — more general data can be accommodated by an appropriate translation, rotation, and scaling.

Satisfaction of the end–point condition $\mathbf{r}(1) = \mathbf{r}(0) = \mathbf{0}$ yields one real and one complex equation, namely

$$\int_0^1 |\boldsymbol{\alpha}(t)|^2 - |\boldsymbol{\beta}(t)|^2 \, \mathrm{d}t = 0 \quad \text{and} \quad \int_0^1 2 \, \boldsymbol{\alpha}(t) \, \overline{\boldsymbol{\beta}}(t) \, \mathrm{d}t = 0 , \tag{6}$$

while imposing the arc length $S = 1$ results in the real equation

$$\int_0^1 |\boldsymbol{\alpha}(t)|^2 + |\boldsymbol{\beta}(t)|^2 \, \mathrm{d}t = 1 . \tag{7}$$

The equations (6)–(7) are equivalent to the simpler system

$$\int_0^1 |\boldsymbol{\alpha}(t)|^2 \, \mathrm{d}t = \int_0^1 |\boldsymbol{\beta}(t)|^2 \, \mathrm{d}t = \tfrac{1}{2} , \quad \int_0^1 \boldsymbol{\alpha}(t) \, \overline{\boldsymbol{\beta}}(t) \, \mathrm{d}t = 0 . \tag{8}$$

Remark 1. The basic C^0 closed–loop problem for PH curves characterized by equations (8) may be phrased in terms of an inner product for complex polynomials, and the induced norm and metric functions. For two complex polynomials $\boldsymbol{\alpha}(t), \boldsymbol{\beta}(t)$ on $t \in [0, 1]$ we define the inner product

$$\langle \boldsymbol{\alpha}, \boldsymbol{\beta} \rangle := \int_0^1 \boldsymbol{\alpha}(t) \, \overline{\boldsymbol{\beta}}(t) \, \mathrm{d}t ,$$

and $\boldsymbol{\alpha}(t), \boldsymbol{\beta}(t)$ are said to be *orthogonal* if $\langle \boldsymbol{\alpha}, \boldsymbol{\beta} \rangle = 0$. Correspondingly, the norms of $\boldsymbol{\alpha}(t), \boldsymbol{\beta}(t)$ are defined as

$$\|\boldsymbol{\alpha}\| := \sqrt{\langle \boldsymbol{\alpha}, \boldsymbol{\alpha} \rangle} , \quad \|\boldsymbol{\beta}\| := \sqrt{\langle \boldsymbol{\beta}, \boldsymbol{\beta} \rangle} ,$$

and the triangle inequality $\|\boldsymbol{\alpha} + \boldsymbol{\beta}\| \leq \|\boldsymbol{\alpha}\| + \|\boldsymbol{\beta}\|$ is satisfied. A metric defining the distance between complex polynomials $\boldsymbol{\alpha}(t), \boldsymbol{\beta}(t)$ may then be specified as

$$\mathrm{distance}(\boldsymbol{\alpha}, \boldsymbol{\beta}) := \|\boldsymbol{\alpha} - \boldsymbol{\beta}\| .$$

4

The system of equations (8) defining a closed–loop spatial PH curve with C^0 continuity can then be succinctly formulated as

$$\|\boldsymbol{\alpha}\| \;=\; \|\boldsymbol{\beta}\| \;=\; \frac{1}{\sqrt{2}}\,, \quad \langle \boldsymbol{\alpha}, \boldsymbol{\beta}\rangle \;=\; 0\,. \tag{9}$$

Since $\|\boldsymbol{\alpha} - \boldsymbol{\beta}\|^2 = \|\boldsymbol{\alpha}\|^2 + \|\boldsymbol{\beta}\|^2 - 2\,\mathrm{Re}(\langle\boldsymbol{\alpha},\boldsymbol{\beta}\rangle)$ these conditions also imply that $\mathrm{distance}(\boldsymbol{\alpha},\boldsymbol{\beta}) = 1$.

Now for the polynomials (5), the integrands in (8) may be formulated in terms of the Bernstein basis of degree 6 on $[\,0,1\,]$ as

$$|\boldsymbol{\alpha}(t)|^2 = |\boldsymbol{\alpha}_0|^2\, b_0^6(t) + \mathrm{Re}(\overline{\boldsymbol{\alpha}}_0\boldsymbol{\alpha}_1)\, b_1^6(t) + \left(\tfrac{2}{5}\mathrm{Re}(\overline{\boldsymbol{\alpha}}_0\boldsymbol{\alpha}_2) + \tfrac{3}{5}|\boldsymbol{\alpha}_1|^2\right) b_2^6(t) + \left(\tfrac{1}{10}\mathrm{Re}(\overline{\boldsymbol{\alpha}}_0\boldsymbol{\alpha}_3) + \tfrac{9}{10}\mathrm{Re}(\overline{\boldsymbol{\alpha}}_1\boldsymbol{\alpha}_2)\right) b_3^6(t)$$

$$+ \left(\tfrac{2}{5}\mathrm{Re}(\overline{\boldsymbol{\alpha}}_1\boldsymbol{\alpha}_3) + \tfrac{3}{5}|\boldsymbol{\alpha}_2|^2\right) b_4^6(t) + \mathrm{Re}(\overline{\boldsymbol{\alpha}}_2\boldsymbol{\alpha}_3)\, b_5^6(t) + |\boldsymbol{\alpha}_3|^2\, b_6^6(t)\,,$$

$$|\boldsymbol{\beta}(t)|^2 = |\boldsymbol{\beta}_0|^2\, b_0^6(t) + \mathrm{Re}(\overline{\boldsymbol{\beta}}_0\boldsymbol{\beta}_1)\, b_1^6(t) + \left(\tfrac{2}{5}\mathrm{Re}(\overline{\boldsymbol{\beta}}_0\boldsymbol{\beta}_2) + \tfrac{3}{5}|\boldsymbol{\beta}_1|^2\right) b_2^6(t) + \left(\tfrac{1}{10}\mathrm{Re}(\overline{\boldsymbol{\beta}}_0\boldsymbol{\beta}_3) + \tfrac{9}{10}\mathrm{Re}(\overline{\boldsymbol{\beta}}_1\boldsymbol{\beta}_2)\right) b_3^6(t)$$

$$+ \left(\tfrac{2}{5}\mathrm{Re}(\overline{\boldsymbol{\beta}}_1\boldsymbol{\beta}_3) + \tfrac{3}{5}|\boldsymbol{\beta}_2|^2\right) b_4^6(t) + \mathrm{Re}(\overline{\boldsymbol{\beta}}_2\boldsymbol{\beta}_3)\, b_5^6(t) + |\boldsymbol{\beta}_3|^2\, b_6^6(t),$$

$$\boldsymbol{\alpha}(t)\,\overline{\boldsymbol{\beta}}(t) = \boldsymbol{\alpha}_0\overline{\boldsymbol{\beta}}_0\, b_0^6(t) + \tfrac{1}{2}\left(\boldsymbol{\alpha}_0\overline{\boldsymbol{\beta}}_1 + \boldsymbol{\alpha}_1\overline{\boldsymbol{\beta}}_0\right) b_1^6(t) + \tfrac{1}{5}\left(\boldsymbol{\alpha}_0\overline{\boldsymbol{\beta}}_2 + \boldsymbol{\alpha}_2\overline{\boldsymbol{\beta}}_0 + 3\,\boldsymbol{\alpha}_1\overline{\boldsymbol{\beta}}_1\right) b_2^6(t)$$

$$+ \tfrac{1}{20}\left(\boldsymbol{\alpha}_0\overline{\boldsymbol{\beta}}_3 + \boldsymbol{\alpha}_3\overline{\boldsymbol{\beta}}_0 + 9\,(\boldsymbol{\alpha}_1\overline{\boldsymbol{\beta}}_2 + \boldsymbol{\alpha}_2\overline{\boldsymbol{\beta}}_1)\right) b_3^6(t) + \tfrac{1}{5}\left(\boldsymbol{\alpha}_1\overline{\boldsymbol{\beta}}_3 + \boldsymbol{\alpha}_3\overline{\boldsymbol{\beta}}_1 + 3\,\boldsymbol{\alpha}_2\overline{\boldsymbol{\beta}}_2\right) b_4^6(t)$$

$$+ \tfrac{1}{2}\left(\boldsymbol{\alpha}_2\overline{\boldsymbol{\beta}}_3 + \boldsymbol{\alpha}_3\overline{\boldsymbol{\beta}}_2\right) b_5^6(t) + \boldsymbol{\alpha}_3\overline{\boldsymbol{\beta}}_3\, b_6^6(t).$$

Since the definite integral of a degree n polynomial over $[\,0,1\,]$ is the sum of its Bernstein coefficients divided by $n + 1$, the equations (8) reduce to

$$10\,|\boldsymbol{\alpha}_0|^2 + 10\,\mathrm{Re}(\overline{\boldsymbol{\alpha}}_0\boldsymbol{\alpha}_1) + 6\,|\boldsymbol{\alpha}_1|^2 + 4\mathrm{Re}(\overline{\boldsymbol{\alpha}}_0\boldsymbol{\alpha}_2) + \mathrm{Re}(\overline{\boldsymbol{\alpha}}_0\boldsymbol{\alpha}_3) + 9\,\mathrm{Re}(\overline{\boldsymbol{\alpha}}_1\boldsymbol{\alpha}_2)$$

$$+ 4\,\mathrm{Re}(\overline{\boldsymbol{\alpha}}_1\boldsymbol{\alpha}_3) + 6\,|\boldsymbol{\alpha}_2|^2 + 10\,\mathrm{Re}(\overline{\boldsymbol{\alpha}}_2\boldsymbol{\alpha}_3) + 10\,|\boldsymbol{\alpha}_3|^2 = 35\,, \tag{10}$$

$$10\,|\boldsymbol{\beta}_0|^2 + 10\,\mathrm{Re}(\overline{\boldsymbol{\beta}}_0\boldsymbol{\beta}_1) + 6\,|\boldsymbol{\beta}_1|^2 + 4\,\mathrm{Re}(\overline{\boldsymbol{\beta}}_0\boldsymbol{\beta}_2) + \mathrm{Re}(\overline{\boldsymbol{\beta}}_0\boldsymbol{\beta}_3) + 9\,\mathrm{Re}(\overline{\boldsymbol{\beta}}_1\boldsymbol{\beta}_2)$$

$$+ 4\,\mathrm{Re}(\overline{\boldsymbol{\beta}}_1\boldsymbol{\beta}_3) + 6\,|\boldsymbol{\beta}_2|^2 + 10\,\mathrm{Re}(\overline{\boldsymbol{\beta}}_2\boldsymbol{\beta}_3) + 10\,|\boldsymbol{\beta}_3|^2 = 35\,, \tag{11}$$

$$20\,\boldsymbol{\alpha}_0\overline{\boldsymbol{\beta}}_0 + 10(\boldsymbol{\alpha}_0\overline{\boldsymbol{\beta}}_1 + \boldsymbol{\alpha}_1\overline{\boldsymbol{\beta}}_0) + 12\,\boldsymbol{\alpha}_1\overline{\boldsymbol{\beta}}_1 + 4(\boldsymbol{\alpha}_0\overline{\boldsymbol{\beta}}_2 + \boldsymbol{\alpha}_2\overline{\boldsymbol{\beta}}_0 + \boldsymbol{\alpha}_1\overline{\boldsymbol{\beta}}_3 + \boldsymbol{\alpha}_3\overline{\boldsymbol{\beta}}_1)$$

$$+ (\boldsymbol{\alpha}_0\overline{\boldsymbol{\beta}}_3 + \boldsymbol{\alpha}_3\overline{\boldsymbol{\beta}}_0) + 9\,(\boldsymbol{\alpha}_1\overline{\boldsymbol{\beta}}_2 + \boldsymbol{\alpha}_2\overline{\boldsymbol{\beta}}_1) + 12\,\boldsymbol{\alpha}_2\overline{\boldsymbol{\beta}}_2 + 10(\boldsymbol{\alpha}_2\overline{\boldsymbol{\beta}}_3 + \boldsymbol{\alpha}_3\overline{\boldsymbol{\beta}}_2) + 20\,\boldsymbol{\alpha}_3\overline{\boldsymbol{\beta}}_3 = 0\,. \tag{12}$$

Now to match the end derivatives we set $\mathbf{r}'(1) = \mathbf{r}'(0) = w^2\,\mathbf{i}$, and we must have

$$\boldsymbol{\alpha}_0 = w\,\mathrm{e}^{\mathrm{i}\,\psi_0}\,, \quad \boldsymbol{\beta}_0 = 0\,, \quad \boldsymbol{\alpha}_3 = w\,\mathrm{e}^{\mathrm{i}\,\psi_3}\,, \quad \boldsymbol{\beta}_3 = 0\,, \tag{13}$$

5

where ψ_0 and ψ_3 are free parameters. Thus, setting $\Delta\psi := \psi_3 - \psi_0$, equations (10)–(12) become

$$(20 + \cos\Delta\psi)\, w^2 \,+\, 6\,|\boldsymbol{\alpha}_1|^2 \,+\, 6\,|\boldsymbol{\alpha}_2|^2 \,+\, 10\,\mathrm{Re}(\overline{\boldsymbol{\alpha}}_0\boldsymbol{\alpha}_1) \,+\, 10\,\mathrm{Re}(\overline{\boldsymbol{\alpha}}_2\boldsymbol{\alpha}_3) \,+\, 4\,\mathrm{Re}(\overline{\boldsymbol{\alpha}}_0\boldsymbol{\alpha}_2)$$

$$+\, 4\,\mathrm{Re}(\overline{\boldsymbol{\alpha}}_1\boldsymbol{\alpha}_3) \,+\, 9\,\mathrm{Re}(\overline{\boldsymbol{\alpha}}_1\boldsymbol{\alpha}_2) \,=\, 35\,, \tag{14}$$

$$6\,|\boldsymbol{\beta}_1|^2 \,+\, 9\,\mathrm{Re}(\overline{\boldsymbol{\beta}}_1\boldsymbol{\beta}_2) \,+\, 6\,|\boldsymbol{\beta}_2|^2 \,=\, 35, \tag{15}$$

$$(10\,\boldsymbol{\alpha}_0 + 12\,\boldsymbol{\alpha}_1 + 9\,\boldsymbol{\alpha}_2 + 4\,\boldsymbol{\alpha}_3)\,\overline{\boldsymbol{\beta}}_1 \,+\, (4\,\boldsymbol{\alpha}_0 + 9\,\boldsymbol{\alpha}_1 + 12\,\boldsymbol{\alpha}_2 + 10\,\boldsymbol{\alpha}_3)\,\overline{\boldsymbol{\beta}}_2 \,=\, 0. \tag{16}$$

The two real equations (14)–(15) and one complex equation (16) impose 4 scalar constraints on the 11 degrees of freedom embodied in $w, \psi_0, \psi_3, \boldsymbol{\alpha}_1, \boldsymbol{\beta}_1, \boldsymbol{\alpha}_2, \boldsymbol{\beta}_2$. Thus, the degree 7 C^1 PH closed loops incorporate 7 free parameters.

3. Imposition of C^2 continuity

The C^1 PH quintic closed loops formulated in [9] exhibit tangent, curvature, and torsion continuity at the juncture point $\mathbf{r}(1) = \mathbf{r}(0)$, but not continuity of the normal and binormal vectors, since continuity of the Frenet frame requires C^2 continuity. We now consider imposing the condition $\mathbf{r}''(1) = \mathbf{r}''(0)$ for C^2 closed loops defined by degree 7 PH curves $\mathbf{r}(t)$. This ensures continuity of the Frenet frame and curvature at $\mathbf{r}(1) = \mathbf{r}(0)$, but not the torsion.

The end–point second derivatives of $\mathbf{r}(t)$ may be expressed as

$$\mathbf{r}''(0) \,=\, 6\,(\mathrm{Re}(\boldsymbol{\alpha}_0\overline{\boldsymbol{\alpha}}_1 - \boldsymbol{\beta}_0\overline{\boldsymbol{\beta}}_1) - |\boldsymbol{\alpha}_0|^2 + |\boldsymbol{\beta}_0|^2, \boldsymbol{\alpha}_0\overline{\boldsymbol{\beta}}_1 + \boldsymbol{\alpha}_1\overline{\boldsymbol{\beta}}_0 - 2\,\boldsymbol{\alpha}_0\overline{\boldsymbol{\beta}}_0)\,,$$

$$\mathbf{r}''(1) \,=\, -\,6\,(\mathrm{Re}(\overline{\boldsymbol{\alpha}}_2\boldsymbol{\alpha}_3 - \overline{\boldsymbol{\beta}}_2\boldsymbol{\beta}_3) - |\boldsymbol{\alpha}_3|^2 + |\boldsymbol{\beta}_3|^2, \boldsymbol{\alpha}_2\overline{\boldsymbol{\beta}}_3 + \boldsymbol{\alpha}_3\overline{\boldsymbol{\beta}}_2 - 2\,\boldsymbol{\alpha}_3\overline{\boldsymbol{\beta}}_3)\,.$$

With $\boldsymbol{\beta}_0 = \boldsymbol{\beta}_3 = 0$ from (13) these expressions simplify to

$$\mathbf{r}''(0) \,=\, 6\,(\mathrm{Re}(\boldsymbol{\alpha}_0\overline{\boldsymbol{\alpha}}_1) - |\boldsymbol{\alpha}_0|^2, \boldsymbol{\alpha}_0\overline{\boldsymbol{\beta}}_1), \quad \mathbf{r}''(1) \,=\, -\,6\,(\mathrm{Re}(\overline{\boldsymbol{\alpha}}_2\boldsymbol{\alpha}_3) - |\boldsymbol{\alpha}_3|^2, \boldsymbol{\alpha}_3\overline{\boldsymbol{\beta}}_2)\,,$$

and on substituting for $\boldsymbol{\alpha}_0, \boldsymbol{\alpha}_3$ from (13) with $w \neq 0$, satisfaction of the C^2 continuity condition $\mathbf{r}''(1) = \mathbf{r}''(0)$ yields the equations

$$\mathrm{Re}(\mathrm{e}^{\mathrm{i}\,\psi_0}\,\overline{\boldsymbol{\alpha}}_1 + \mathrm{e}^{\mathrm{i}\,\psi_3}\,\overline{\boldsymbol{\alpha}}_2) \,=\, 2\,w\,, \tag{17}$$

$$\mathrm{e}^{\mathrm{i}\,\psi_0}\,\overline{\boldsymbol{\beta}}_1 + \mathrm{e}^{\mathrm{i}\,\psi_3}\,\overline{\boldsymbol{\beta}}_2 \,=\, 0\,. \tag{18}$$

Equation (18) indicates that $\boldsymbol{\beta}_1, \boldsymbol{\beta}_2$ can be written in terms of free parameters $\lambda > 0$ and $\phi \in [\,0, 2\pi)$ as

$$\boldsymbol{\beta}_1 \,=\, \lambda\,\mathrm{e}^{\mathrm{i}(\psi_0 + \phi)}\,, \quad \boldsymbol{\beta}_2 \,=\, -\lambda\,\mathrm{e}^{\mathrm{i}(\psi_3 + \phi)}\,. \tag{19}$$

6

Equation (15) is then satisfied if λ is given in terms of $\Delta\psi = \psi_3 - \psi_0$ by

$$\lambda = \sqrt{\frac{35}{12 - 9\cos\Delta\psi}}\,. \tag{20}$$

Now since $(\boldsymbol{\beta}_0, \boldsymbol{\beta}_1, \boldsymbol{\beta}_2, \boldsymbol{\beta}_3) = \lambda\,\mathrm{e}^{\mathrm{i}\,\phi}(0, \mathrm{e}^{\mathrm{i}\,\psi_0}, -\mathrm{e}^{\mathrm{i}\,\psi_3}, 0)$ the polynomial $\boldsymbol{\beta}(t)$, when $\phi \neq 0$, is simply its instance when $\phi = 0$ multiplied by the factor $\mathrm{e}^{\mathrm{i}\,\phi}$. This factor does not change the hodograph component $x'(t) = |\boldsymbol{\alpha}(t)|^2 - |\boldsymbol{\beta}(t)|^2$, while $y'(t) + \mathrm{i}\,z'(t)$ is modified from $2\,\boldsymbol{\alpha}(t)\overline{\boldsymbol{\beta}}(t)$ to $2\,\boldsymbol{\alpha}(t)\overline{\boldsymbol{\beta}}(t)\,\mathrm{e}^{-\mathrm{i}\,\phi}$ so $y'(t)$ becomes $\cos\phi\,y'(t) + \sin\phi\,z'(t)$ and $z'(t)$ becomes $-\sin\phi\,y'(t) + \cos\phi\,z'(t)$. Since this simply represents a rotation of the hodograph $\mathbf{r}'(t)$ determined with $\phi = 0$ about the x–axis, we henceforth focus on the case $\phi = 0$.

Using (19) with $\phi = 0$ and substituting $\boldsymbol{\alpha}_1 = w\,\mathbf{a}_1\,\mathrm{e}^{\mathrm{i}\,\psi_0}$ and $\boldsymbol{\alpha}_2 = w\,\mathbf{a}_2\,\mathrm{e}^{\mathrm{i}\,\psi_3}$ into equations (14), (16), and (17), we obtain

$$w^2\,[\,20\,+\,\cos\Delta\psi\,+\,6\,(|\mathbf{a}_1|^2 + |\mathbf{a}_2|^2)\,+\,10\,\mathrm{Re}(\mathbf{a}_1 + \overline{\mathbf{a}}_2)$$
$$+\,4\,\mathrm{Re}(\overline{\mathbf{a}}_1\mathrm{e}^{\mathrm{i}\Delta\psi} + \mathbf{a}_2\mathrm{e}^{\mathrm{i}\Delta\psi})\,+\,9\,\mathrm{Re}(\overline{\mathbf{a}}_1\mathbf{a}_2\mathrm{e}^{\mathrm{i}\,\Delta\psi})\,]\,=\,35\,, \tag{21}$$

$$(12 - 9\,\mathrm{e}^{-\mathrm{i}\,\Delta\psi})\,\mathbf{a}_1\,+\,(9\,\mathrm{e}^{\mathrm{i}\,\Delta\psi} - 12)\,\mathbf{a}_2\,=\,-8\sin\Delta\psi\,\mathrm{i}\,, \tag{22}$$

$$\mathrm{Re}(\overline{\mathbf{a}}_1 + \overline{\mathbf{a}}_2)\,=\,2\,. \tag{23}$$

Re–writing equation (23) as

$$\mathbf{a}_1 + \mathbf{a}_2\,=\,2 + \xi\,\mathrm{i}\,, \tag{24}$$

where ξ is a free real parameter, we may solve it simultaneously with equation (22) to obtain $\mathbf{a}_1, \mathbf{a}_2$ in terms of $\Delta\psi, \xi$ as

$$\mathbf{a}_1\,=\,\frac{(12 - 9\,\mathrm{e}^{\mathrm{i}\Delta\psi})(2 + \xi\,\mathrm{i}) - 8\sin\Delta\psi\,\mathrm{i}}{24 - 18\cos\Delta\psi}\,, \tag{25}$$

$$\mathbf{a}_2\,=\,\frac{(12 - 9\,\mathrm{e}^{-\mathrm{i}\Delta\psi})(2 + \xi\,\mathrm{i}) + 8\sin\Delta\psi\,\mathrm{i}}{24 - 18\cos\Delta\psi}\,. \tag{26}$$

Finally, substituting these expressions for $\mathbf{a}_1, \mathbf{a}_2$ into equation (21) identifies, for each choice of $\Delta\psi$ and ξ, the unique positive value of w in (13) as

$$w\,=\,\frac{2\sqrt{15\,c_0}}{\sqrt{260 - 144\cos\Delta\psi + 4\cos^2\Delta\psi + 9\,\xi^2}}\,, \tag{27}$$

where we set

$$c_0\,:=\,4 - 3\cos\Delta\psi\,. \tag{28}$$

7

Lemma 1. *The hodograph* (4) *depends only on the difference* $\Delta\psi = \psi_3 - \psi_0$ *of the angles* ψ_0, ψ_3 *in* (13).

Proof : The coefficients

$$(\boldsymbol{\alpha}_0, \boldsymbol{\alpha}_1, \boldsymbol{\alpha}_2, \boldsymbol{\alpha}_3) = (w\,\mathrm{e}^{\mathrm{i}\,\psi_0}, w\,\mathbf{a}_1\,\mathrm{e}^{\mathrm{i}\,\psi_0}, w\,\mathbf{a}_2\,\mathrm{e}^{\mathrm{i}\,\psi_3}, \mathrm{e}^{\mathrm{i}\,\psi_3}) \quad \text{and} \quad (\boldsymbol{\beta}_0, \boldsymbol{\beta}_1, \boldsymbol{\beta}_2, \boldsymbol{\beta}_3) = (0, \lambda\,\mathrm{e}^{\mathrm{i}\,\psi_0}, -\lambda\,\mathrm{e}^{\mathrm{i}\,\psi_3}, 0)$$

of $\boldsymbol{\alpha}(t)$ and $\boldsymbol{\beta}(t)$, as determined above, may be expressed as

$$(\boldsymbol{\alpha}_0, \boldsymbol{\alpha}_1, \boldsymbol{\alpha}_2, \boldsymbol{\alpha}_3) = \mathrm{e}^{\mathrm{i}\,\psi_0}\,w\,(1, \mathbf{a}_1, \mathbf{a}_2\,\mathrm{e}^{\mathrm{i}\,\Delta\psi}, \mathrm{e}^{\mathrm{i}\,\Delta\psi}), \tag{29}$$

$$(\boldsymbol{\beta}_0, \boldsymbol{\beta}_1, \boldsymbol{\beta}_2, \boldsymbol{\beta}_3) = \mathrm{e}^{\mathrm{i}\,\psi_0}\,\lambda\,(0, 1, -\mathrm{e}^{\mathrm{i}\,\Delta\psi}, 0), \tag{30}$$

where $\lambda, \mathbf{a}_1, \mathbf{a}_2, w$ — as defined by (20) and (25)–(27) — depend only on $\Delta\psi$. On forming the expressions $|\boldsymbol{\alpha}(t)|^2 - |\boldsymbol{\beta}(t)|^2$ and $2\,\boldsymbol{\alpha}(t)\overline{\boldsymbol{\beta}}(t)$ in (4), the factors $\mathrm{e}^{\mathrm{i}\,\psi_0}$ extracted from $\boldsymbol{\alpha}(t)$ and $\boldsymbol{\beta}(t)$ vanish, so $\mathbf{r}'(t)$ depends only on $\Delta\psi$. $\blacksquare$

In view of the above, we henceforth set $\psi_0 = 0$ and $\psi_3 = \psi \in (-\pi, \pi]$ so that $\Delta\psi = \psi$. We may summarize the preceding results as follows.

Theorem 1. *The degree 7 canonical–form C^2 PH curve closed loops comprise a two–parameter family, dependent on the parameters ξ and ψ. For each instance of the parameters, a unique closed–form solution is obtained by substituting the coefficients* (29)–(30) *into* (5) *and integrating* (4)*, where $\lambda, \mathbf{a}_1, \mathbf{a}_2, w$ are defined by* (20) *and* (25)–(27)*.*

Remark 2. It is useful to note some specializations of the expressions (25) and (26) with respect to ξ and ψ. First, when $\xi = 0$ we have

$$\mathbf{a}_1 = 1 - \frac{13\sin\psi}{12 - 9\cos\psi}\,\mathrm{i}, \quad \mathbf{a}_2 = 1 + \frac{13\sin\psi}{12 - 9\cos\psi}\,\mathrm{i}.$$

Second, if $\psi = 0$ or π we obtain

$$\mathbf{a}_1 = \mathbf{a}_2 = \frac{2 + \xi\,\mathrm{i}}{2}.$$

Finally, when $\xi = 0$ and $\psi = 0$ or π we have simply $\mathbf{a}_1 = \mathbf{a}_2 = 1$, and this implies that $\mathbf{r}(t)$ degenerates to a planar curve (see Lemma 3 below). Recall that the C^1 closed–loop PH quintics constructed in [9] also degenerate to planar curves when $\psi = 0$ or π.

The end–point third derivatives of $\mathbf{r}(t)$ can be expressed as

$$\mathbf{r}'''(0) = 6\,(\,5\,(|\boldsymbol{\alpha}_0|^2 - |\boldsymbol{\beta}_0|^2) + 3\,(|\boldsymbol{\alpha}_1|^2 - |\boldsymbol{\beta}_1|^2) - 10\,\mathrm{Re}(\boldsymbol{\alpha}_0\overline{\boldsymbol{\alpha}}_1 - \boldsymbol{\beta}_0\overline{\boldsymbol{\beta}}_1) + 2\,\mathrm{Re}(\boldsymbol{\alpha}_0\overline{\boldsymbol{\alpha}}_2 - \boldsymbol{\beta}_0\overline{\boldsymbol{\beta}}_2)\,,$$
$$10\,(\boldsymbol{\alpha}_0\overline{\boldsymbol{\beta}}_0 - \boldsymbol{\alpha}_1\overline{\boldsymbol{\beta}}_0 - \boldsymbol{\alpha}_0\overline{\boldsymbol{\beta}}_1) + 2\,(\boldsymbol{\alpha}_2\overline{\boldsymbol{\beta}}_0 + \boldsymbol{\alpha}_0\overline{\boldsymbol{\beta}}_2) + 6\,\boldsymbol{\alpha}_1\overline{\boldsymbol{\beta}}_1\,)\,,$$

$$\mathbf{r}'''(1) = 6\,(\,5\,(|\boldsymbol{\alpha}_3|^2 - |\boldsymbol{\beta}_3|^2) + 3\,(|\boldsymbol{\alpha}_2|^2 - |\boldsymbol{\beta}_2|^2) - 10\,\mathrm{Re}(\boldsymbol{\alpha}_2\overline{\boldsymbol{\alpha}}_3 - \boldsymbol{\beta}_2\overline{\boldsymbol{\beta}}_3) + 2\,\mathrm{Re}(\boldsymbol{\alpha}_1\overline{\boldsymbol{\alpha}}_3 - \boldsymbol{\beta}_1\overline{\boldsymbol{\beta}}_3)\,,$$
$$10\,(\boldsymbol{\alpha}_3\overline{\boldsymbol{\beta}}_3 - \boldsymbol{\alpha}_2\overline{\boldsymbol{\beta}}_3 - \boldsymbol{\alpha}_3\overline{\boldsymbol{\beta}}_2) + 2\,(\boldsymbol{\alpha}_1\overline{\boldsymbol{\beta}}_3 + \boldsymbol{\alpha}_3\overline{\boldsymbol{\beta}}_1) + 6\,\boldsymbol{\alpha}_2\overline{\boldsymbol{\beta}}_2\,)\,.$$

8

The C^3 condition $\mathbf{r}'''(1) = \mathbf{r}'''(0)$ is a vector constraint that cannot, in general, be satisfied by C^2 closed–loop PH
curves of degree 7 because they have only two residual free parameters. However, proceeding to degree 9 PH curves
yields four new degrees of freedom, and it may then be possible to construct C^3 spatial closed loops with prescribed
arc lengths and continuity of the position, Frenet frame, curvature, torsion, and arc–length derivative of curvature.

4. Properties of the C^2 closed loops

For the C^2 closed–loop PH curves constructed from the coefficients (29)–(30) specified by (20) and (25)–(27), the control points of the Bézier form

$$\mathbf{r}(t) = \sum_{i=0}^{7} \mathbf{p}_i b_i^7(t) \tag{31}$$

can be expressed as

$$\mathbf{p}_0 = \mathbf{p}_7 = (\,0,0,0\,), \quad \mathbf{p}_1 = \frac{1}{7}\,(\,w^2,0,0\,), \quad \mathbf{p}_6 = -\frac{1}{7}\,(\,w^2,0,0\,),$$

$$\mathbf{p}_2 = \frac{1}{7}\left(\,2\,w^2\left(1 + \frac{3\,\xi\sin\psi}{4\,c_0}\right), \sqrt{\frac{35}{3\,c_0}}\,w, 0\,\right), \quad \mathbf{p}_5 = \frac{1}{7}\left(\,2\,w^2\left(-1 + \frac{3\,\xi\sin\psi}{4\,c_0}\right), \sqrt{\frac{35}{3\,c_0}}\,w, 0\,\right),$$

$$\mathbf{p}_3 = \frac{w}{\sqrt{105}\,c_0^{3/2}} \begin{bmatrix} \sqrt{\dfrac{3}{35\,c_0}}\,\dfrac{w}{4}\,(c_1 - 2\,c_0\xi\sin\psi + c_2\xi^2) \\[2mm] 47 - 41\cos\psi + 3\cos 2\psi + 9\,\xi\sin\psi \\[2mm] 3\,c_0\xi - 18\sin\psi - 3\sin 2\psi \end{bmatrix}^T,$$

$$\mathbf{p}_4 = \frac{w}{\sqrt{105}\,c_0^{3/2}} \begin{bmatrix} \sqrt{\dfrac{3}{35\,c_0}}\,\dfrac{w}{4}\,(-c_1 - 2\,c_0\xi\sin\psi - c_2\xi^2) \\[2mm] 47 - 41\cos\psi + 3\cos 2\psi - 9\,\xi\sin\psi \\[2mm] 3\,c_0\xi + 18\sin\psi + 3\sin 2\psi \end{bmatrix}^T, \tag{32}$$

where c_0 is given by (28), and we define

$$c_1 := 4\,[\,78 - 8\cos^3\psi + 45\cos^2\psi - 170\cos\psi\,], \quad c_2 := 18\,[\,3 - 4\cos\psi\,].$$

4.1. Regularity of the closed loops

We may verify the regularity of the C^2 closed–loop PH curves $\mathbf{r}(t)$ as follows. From (4), irregular points with $\mathbf{r}'(t) = \mathbf{0}$ can occur if and only if $\boldsymbol{\alpha}(t)$ and $\boldsymbol{\beta}(t)$ have a common root. Using (5) and (30) with $\psi_0 = 0$ and $\Delta\psi = \psi$, the complex polynomial $\boldsymbol{\beta}(t)$ can be written as

$$\boldsymbol{\beta}(t) = 3\,\lambda\,(1-t)t\,[\,1 - t - t\cos\psi - \mathrm{i}\,t\sin\psi\,].$$

9

Consequently, $\boldsymbol{\beta}(t)$ vanishes if and only if $t = 0$ or 1, or $t = \frac{1}{2}$ when $\psi = 0$. Now from (5), (24), and (29), we have

$$\boldsymbol{\alpha}(0) \,=\, w\,, \quad \boldsymbol{\alpha}(1) \,=\, w\,e^{\mathrm{i}\psi}\,, \quad \boldsymbol{\alpha}(\tfrac{1}{2})\big|_{\psi=0} \,=\, w\left(1+\mathrm{i}\,\frac{3}{8}\,\xi\right).$$

Since $\xi \in (-\infty, \infty)$ equation (27) implies that $w \neq 0$, so $\boldsymbol{\alpha}(t)$, $\boldsymbol{\beta}(t)$ cannot have a common root. Hence, the curve $\mathbf{r}(t)$ is regular.

4.2. Symmetry properties

Careful inspection of the control point expressions (32) reveals some possible symmetry or antisymmetry properties of the C^2 closed–loop PH curves $\mathbf{r}(t) = (x(t), y(t), z(t))$ and their derivatives over the interval $t \in [\,0, 1\,]$. For certain values of the parameters ξ and ψ, these properties are expressed by relations of the form

$$\mathbf{r}^{(\ell)}(t) \,=\, \mathbf{r}^{(\ell)}(1 - t)\,\mathrm{diag}\,(\pm 1, \pm 1, \pm 1)\,, \quad \ell \geq 0\,, \tag{33}$$

where $\mathrm{diag}\,(\pm 1, \pm 1, \pm 1)$ is a 3×3 diagonal matrix whose non–zero elements are -1 or $+1$. Comparing $\mathbf{p}_1$ and $\mathbf{p}_6$ with $w \neq 0$ indicates that $x(t)$ can only be antisymmetric, while $\mathbf{p}_2$ and $\mathbf{p}_5$ indicate that $y(t)$ can only be symmetric. A careful consideration of the dependence of all the control points $\mathbf{p}_0, \ldots, \mathbf{p}_7$ on ξ and ψ yields the following comprehensive characterization.

Lemma 2. *The C^2 closed–loop PH curve* (31) *specified by the control points* (32) *and its derivatives satisfy, for $\ell \geq 0$, the relations*

(1) $\mathbf{r}^{(\ell)}(t) \,=\, (-1)^{\ell}\,\mathbf{r}^{(\ell)}(1 - t)\,\mathrm{diag}(-1, 1, -1)$ *if and only if $\xi = 0$,*

(2) $\mathbf{r}^{(\ell)}(t) \,=\, (-1)^{\ell}\,\mathbf{r}^{(\ell)}(1 - t)\,\mathrm{diag}(-1, 1, 1)$ *if and only if $\psi \in \{0, \pi\}$.*

Furthermore, the parametric speed σ and curvature κ are symmetric on $[\,0, 1\,]$, while the torsion τ is symmetric in case (1) and antisymmetric in case (2).

Proof : The proof of (1) and (2) is a direct consequence of the expressions (32) for the control points and the chain rule. The symmetry of σ then follows directly from (1) and (2), while the properties of the curvature and the torsion are consequences of the relations

$$(\mathbf{r}' \times \mathbf{r}'')(t) \,=\, (\mathbf{r}' \times \mathbf{r}'')(1 - t)\,\mathrm{diag}(\pm 1, \pm(-1), 1)\,,$$

where the plus sign corresponds to the case $\xi = 0$ and the minus sign to the case $\psi \in \{0, \pi\}$. ∎

Note that in case (1), with $\xi = 0$, the closed–loop PH curve $\mathbf{r}(t)$ is also continuous in torsion at the juncture point $\mathbf{r}(1) = \mathbf{r}(0)$. We will show below that when $\xi = 0$ *and* $\psi \in \{0, \pi\}$ the curve $\mathbf{r}(t)$ is planar, with $z(t) \equiv 0$ and vanishing torsion, so the results of Lemma 2 still hold. Examples of curves illustrating the properties in Lemma 2 are shown in Figures 1 and 2.
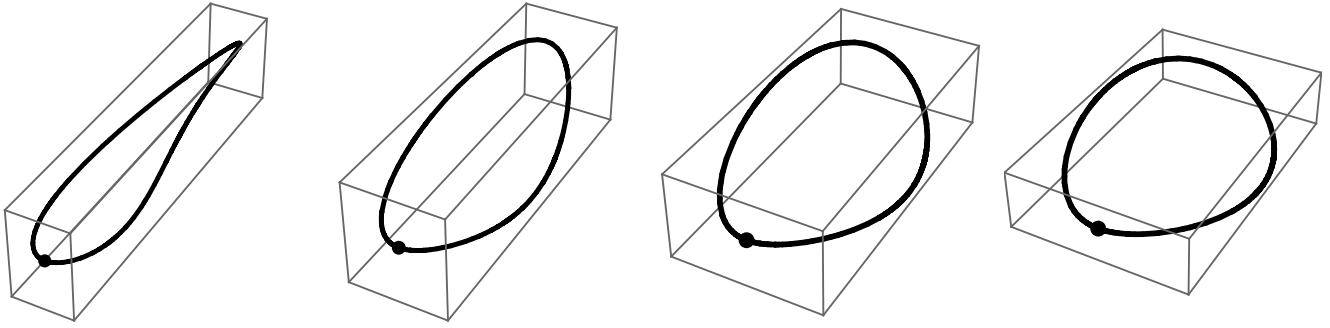
10

Figure 1: The curves $\mathbf{r}(t)$ with $\xi = 0$ and $\psi = k\pi/10$ for $k = 1, 2, 3, 4$.
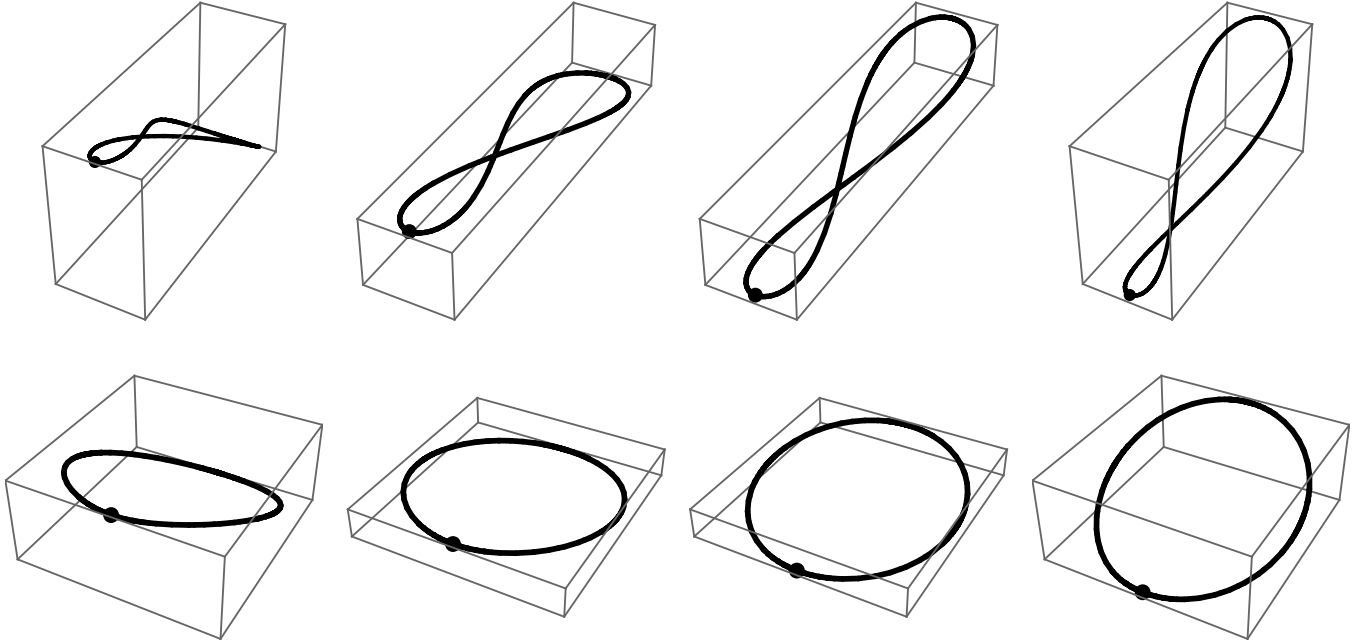

Figure 2: Examples of the C^2 closed–loop curves $\mathbf{r}(t)$ determined by $\psi = 0$ (above) and $\psi = \pi$ (below) for four equidistant values of ξ on $[-2.2, 2.2]$.

4.3. Degeneration to planar curves

For certain special values of the parameters ξ and ψ, the closed loop $\mathbf{r}(t)$ may degenerate to a planar curve. These cases may be characterized as follows.

Lemma 3. *For $(\xi, \psi) \in (-\infty, \infty) \times (-\pi, \pi]$, the only planar instances of the C^2 closed–loop PH curves specified by*

11

the control points (32) *correspond to the values* (i) $\xi = \psi = 0$, *in which case we have*

$$\mathbf{r}(t) \;=\; \left(t\,(1-t)(\tfrac{1}{2}-t)\,p_0(t)\,,\ \sqrt{\frac{105}{2}}\,(1-t)^2 t^2\,,\ 0 \right),$$

where $p_0(t) = -60t^4 + 120t^3 - 63t^2 + 3t + 1$, *and* (ii) $\xi = 0$, $\psi = \pi$ *for which*

$$\mathbf{r}(t) \;=\; \left(\frac{5}{17}\,t\,(1-t)(\tfrac{1}{2}-t)\,p_\pi(t)\,,\ -5\,\sqrt{\frac{7}{102}}\,(1-t)^2 t^2 (2t-3)(2t+1)\,,\ 0 \right),$$

89   *with* $p_\pi(t) = 8t^4 - 16t^3 - 13t^2 + 21t + 7$. *Both curves have antisymmetric* x *components, and symmetric* y *components.*

90   *For* $t \in (0,1)$ *the curve* $\mathbf{r}(t)$ *has one self–intersection in case* (i), *and is free of self–intersections in case* (ii).

Proof :   For $\xi = 0$ and $\psi \in \{0,\pi\}$, the quantities (25)–(26) reduce to

$$\mathbf{a}_1 \;=\; \mathbf{a}_2 \;=\; 1\,.$$

Consequently, $\boldsymbol{\alpha}(t)$ and $\boldsymbol{\beta}(t)$ have coefficients of the form

$$(\boldsymbol{\alpha}_0, \boldsymbol{\alpha}_1, \boldsymbol{\alpha}_2, \boldsymbol{\alpha}_3) \;=\; w\,(1, 1, \mathrm{e}^{\mathrm{i}\,\psi}, \mathrm{e}^{\mathrm{i}\,\psi}) \;=\; w\,(1, 1, \pm 1, \pm 1), \quad (\boldsymbol{\beta}_0, \boldsymbol{\beta}_1, \boldsymbol{\beta}_2, \boldsymbol{\beta}_3) \;=\; \lambda\,(0, 1, -\mathrm{e}^{\mathrm{i}\,\psi}, 0) \;=\; \lambda\,(0, 1, \mp 1, 0)\,.$$

91   Hence $\boldsymbol{\alpha}(t) = a(t)$, $\boldsymbol{\beta}(t) = b(t)$ for *real* polynomials $a(t)$, $b(t)$ and $\mathbf{r}'(t)$ has components $x'(t) = a^2(t) - b^2(t)$,

92   $y'(t) = 2\,a(t)b(t)$, $z'(t) = 0$ when $\xi = 0$ and $\psi = 0$ or π. Therefore, $\mathbf{r}(t)$ is a planar curve.

Conversely, when $\mathbf{r}(t)$ is a planar curve, its torsion must satisfy $\tau(t) \equiv 0$. By straightforward computations, we have

$$\tau(0) \;=\; [\,(3\cos\psi - 4)\xi + 6\sin\psi + \sin 2\psi\,]\,f(\xi,\psi)\,, \tag{34}$$

$$\tau(1) \;=\; [\,(4 - 3\cos\psi)\xi + 6\sin\psi + \sin 2\psi\,]\,f(\xi,\psi)\,, \tag{35}$$

where for $(\xi,\psi) \in (-\infty, \infty) \times (-\pi, \pi\,]$ we have

$$f(\xi,\psi) \;:=\; -\,\frac{(260 - 144\cos\psi + 4\cos^2\psi + 9\,\xi^2)}{20\,(4 - 3\cos\psi)^2} \;<\; 0\,.$$

Now from (34), the condition $\tau(0) = 0$ implies that

$$\xi \;=\; \xi_* \;:=\; 2\sin\psi\,\frac{3 + \cos\psi}{4 - 3\cos\psi}\,. \tag{36}$$

Substituting (36) into (35) leads to

$$\tau(1) \;=\; 4\,\sin\psi\,(3 + \cos\psi)\,f(\xi_*, \psi)\,.$$

93   Hence, since $\tau(1) = 0$ and $f(\xi_*, \psi) < 0$, we must have $\psi = 0$ or $\psi = \pi$, and from (36) this implies that $\xi = 0$.

12

The curve symmetry properties now follow directly from Lemma 2, and as a consequence self–intersection points on $(0, 1)$ can lie only on the y–axis. To identify them, we must study the real roots of $p_0(t)$ and $p_\pi(t)$. One can easily verify that $p_0(t)$ has only the two roots t_0 and $1 - t_0$ on $(0, 1)$, where

$$ t_0 = \frac{1}{2} \left[1 - \sqrt{\frac{27 - \sqrt{249}}{30}} \right] \approx 0.1942 \,, $$

while all roots of $p_\pi(t)$ lie outside $[0, 1]$. Since $\mathbf{r}(t_0) = \mathbf{r}(1 - t_0)$ when $\xi = \psi = 0$, the planar curve identified by these values has a self–intersection. ∎
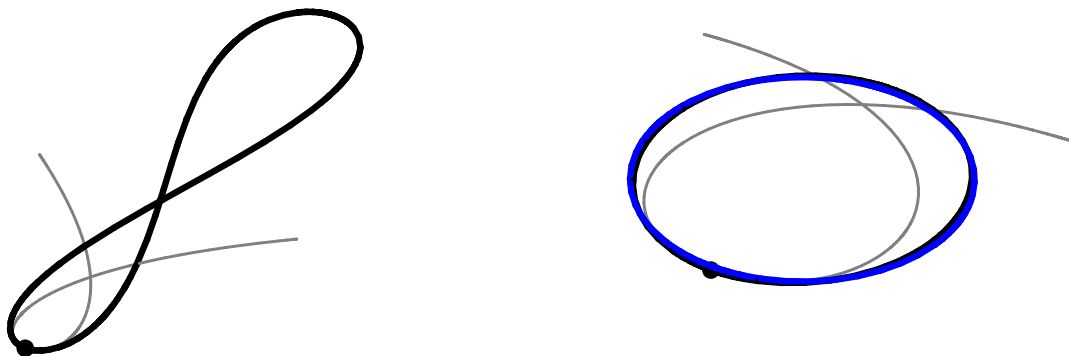
Figure 3: Planar instances of the closed–loop curves $\mathbf{r}(t)$, corresponding to the parameter values $\xi = \psi = 0$ (left), and $\xi = 0$, $\psi = \pi$ (right, black). The latter curve is quite close to a circle of radius $1/2\pi$ (indicated by the blue line). The gray segments indicate portions of the curves for parameter values outside the interval $[0, 1]$.

The two planar instances of the C^2 closed–loop PH curves are illustrated in Figure 3. The case $\xi = 0$, $\psi = \pi$ approximates a uniformly–parameterized circle with center $\mathbf{c} = (0, 1/2\pi)$ and radius $1/2\pi$, satisfying

$$ 0.9649 \le \frac{|\mathbf{r}(t) - \mathbf{c}|}{r} \le 1.0575 \quad \text{and} \quad 0.9375 \le \sigma(t) \le 1.0395 \,. $$

4.4. The $\xi \to \pm\infty$ limit curves

An interesting situation arises when the parameter ξ tends to $\pm\infty$. We focus on the case $\xi \to \infty$, since the case $\xi \to -\infty$ is closely analogous. For each ψ, the limit curve $\mathbf{r}_\infty(t)$ is defined as the locus (31) specified by the limits

13

of the control points (32), with w given by (27), as $\xi \to \infty$.

One can easily see that, in the limit $\xi \to \infty$, the control points $\mathbf{p}_0, \mathbf{p}_1, \mathbf{p}_2$ and $\mathbf{p}_5, \mathbf{p}_6, \mathbf{p}_7$ are coincident at the origin, and by elementary computations we obtain

$$\mathbf{r}_\infty(t) = R_\varphi\, \hat{\mathbf{r}}(t), \tag{37}$$

where $\hat{\mathbf{r}}(t) := 30\,(1-t)^3 t^3\,\left(2\,t - 1, 0, \sqrt{7}/3\,\right)$ and R_φ is a clockwise rotation about the z–axis by the angle

$$\varphi = \arccos \frac{4\cos\psi - 3}{4 - 3\cos\psi}\,.$$

By (37), the curve $\mathbf{r}_\infty(t)$ and its derivatives incorporate the symmetries

$$\mathbf{r}_\infty^{(\ell)}(t) = (-1)^\ell\, \mathbf{r}_\infty^{(\ell)}(1-t)\,\mathrm{diag}(-1, -1, 1)\,, \quad \ell \geq 0\,.$$

The parametric speed and curvature are symmetric, but the torsion vanishes since by (37) the curve $\mathbf{r}_\infty(t)$ is a rotated version of the planar curve $\hat{\mathbf{r}}(t)$ and it must also be planar. Because of the factor $(1-t)^3 t^3$ in $\hat{\mathbf{r}}(t)$, the first and second derivatives of $\mathbf{r}_\infty(t)$ vanish at the juncture point $\mathbf{r}_\infty(1) = \mathbf{r}_\infty(0)$, and the limit curve is irregular at that point.

The limit curve $\mathbf{r}_{-\infty}(t)$ corresponding to the case $\xi \to -\infty$ is obtained by simply applying a composition of reflections of $\mathbf{r}_\infty(t)$ in the (x, y) and (x, z) planes. All of these properties can be seen in Figure 4.

5. Adapted frames on degree 7 C^2 closed–loop PH curves

We now consider the construction of rational adapted orthonormal frames on the C^2 closed–loop PH curves. An *adapted* orthonormal frame $(\mathbf{f}_1(t), \mathbf{f}_2(t), \mathbf{f}_3(t))$ on a space curve $\mathbf{r}(t)$ incorporates the curve tangent $\mathbf{t} = \mathbf{r}'/|\mathbf{r}'|$ as the vector $\mathbf{f}_1$, while $\mathbf{f}_2, \mathbf{f}_3$ span the curve normal plane. The Frenet frame (1) is an adapted frame, but it is not (in general) rational in the curve parameter t. However, every spatial PH curve admits [2] a rational adapted frame, the *Euler–Rodrigues frame* (ERF) with frame vectors $(\mathbf{e}_1(t), \mathbf{e}_2(t), \mathbf{e}_3(t))$ expressed in terms of the two complex polynomials $\boldsymbol{\alpha}(t) = u(t) + \mathrm{i}\,v(t)$ and $\boldsymbol{\beta}(t) = q(t) + \mathrm{i}\,p(t)$ as

$$\begin{aligned}
\mathbf{e}_1 &= \frac{\left(u^2 + v^2 - p^2 - q^2,\, 2(uq + vp),\, 2(vq - up)\right)^T}{u^2 + v^2 + p^2 + q^2}\,, \\
\mathbf{e}_2 &= \frac{\left(2(vp - uq),\, u^2 - v^2 + p^2 - q^2,\, 2(uv + pq)\right)^T}{u^2 + v^2 + p^2 + q^2}\,, \\
\mathbf{e}_3 &= \frac{\left(2(up + vq),\, 2(pq - uv),\, u^2 - v^2 - p^2 + q^2\right)^T}{u^2 + v^2 + p^2 + q^2}\,.
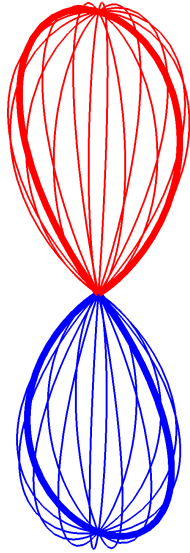\end{aligned} \tag{38}$$

14

Figure 4: The limit curves $\mathbf{r}_\infty(t)$ (red) and $\mathbf{r}_{-\infty}(t)$ (blue) for several choices of the parameter ψ. The bold curves depict the case $\psi = 0$.

Any other rational adapted frame can be obtained from the ERF through a (rational) rotation of $\mathbf{e}_2$ and $\mathbf{e}_3$ in the normal plane.

In the context of closed–loop PH curves, periodic orthonormal frames satisfying $\mathbf{f}_i(1) = \mathbf{f}_i(0)$, $i = 1, 2, 3$, are desired. Since the constructed degree 7 closed–loop PH curves are C^2 continuous, the Frenet frame is periodic, but the ERF is (in general) not periodic — the initial/final normal–plane vectors

$$\mathbf{e}_2(0) = (0, 1, 0)\,, \quad \mathbf{e}_2(1) = (0, \cos(2\psi), \sin(2\psi))\,, \quad \mathbf{e}_3(0) = (0, 0, 1)\,, \quad \mathbf{e}_3(1) = (0, -\sin(2\psi), \cos(2\psi))\,,$$

coincide only when $\psi = k\pi$ for integer k. Note that $\mathbf{e}_2(1), \mathbf{e}_3(1)$ are obtained from $\mathbf{e}_2(0), \mathbf{e}_3(0)$ by a normal–plane rotation through angle 2ψ, i.e.,

$$\begin{bmatrix} \mathbf{e}_2(1) \\ \mathbf{e}_3(1) \end{bmatrix} = \begin{bmatrix} \cos(2\psi) & \sin(2\psi) \\ -\sin(2\psi) & \cos(2\psi) \end{bmatrix} \begin{bmatrix} \mathbf{e}_2(0) \\ \mathbf{e}_3(0) \end{bmatrix}. \tag{39}$$

To construct a periodic rational adapted frame $(\mathbf{f}_1, \mathbf{f}_2, \mathbf{f}_3)$ with $\mathbf{f}_1 = \mathbf{e}_1 = \mathbf{t}$, we must impose a rational normal–plane rotation

$$\begin{bmatrix} \mathbf{f}_2(t) \\ \mathbf{f}_3(t) \end{bmatrix} = \frac{1}{a^2(t) + b^2(t)} \begin{bmatrix} a^2(t) - b^2(t) & 2\,a(t)b(t) \\ -2\,a(t)b(t) & a^2(t) - b^2(t) \end{bmatrix} \begin{bmatrix} \mathbf{e}_2(t) \\ \mathbf{e}_3(t) \end{bmatrix}, \tag{40}$$

15

for relatively prime polynomials $a(t), b(t)$ such that $\mathbf{f}_2(1) = \mathbf{f}_2(0)$, $\mathbf{f}_3(1) = \mathbf{f}_3(0)$. This corresponds to the normal–plane rotation angle $\theta(t) = 2 \tan^{-1}(b(t)/a(t))$. As in [9] we combine $a(t), b(t)$ into a complex polynomial $\mathbf{w}(t) = a(t) + \mathrm{i}\, b(t)$, and consider the simplest case — a linear polynomial $\mathbf{w}(t) = \mathbf{w}_0\,(1 - t) + \mathbf{w}_1\, t$ with $\mathbf{w}_0, \mathbf{w}_1 \in \mathbb{C}$, such that

$$\cos\theta(t) + \mathrm{i}\,\sin\theta(t) = \frac{\mathbf{w}^2(t)}{|\mathbf{w}(t)|^2}. \tag{41}$$

Choosing $\theta_0 = \arg(\mathbf{w}_0)$ and setting $\theta(0) = 2\,\theta_0$, it follows from (39) and (40) that the frame is periodic if and only if $\theta(1) = 2(\theta_0 - \psi) + 2k\pi$ for integer k, which implies that

$$\mathbf{w}_0 = \cos\theta_0 + \mathrm{i}\,\sin\theta_0, \quad \mathbf{w}_1 = \gamma\left(\cos\left(\theta_0 - \psi + k\pi\right) + \mathrm{i}\,\sin\left(\theta_0 - \psi + k\pi\right)\right)$$

for some real constant $\gamma \neq 0$. Henceforth, we also assume that $\theta_0 = 0$, i.e., $\mathbf{f}_2(0) = \mathbf{e}_2(0)$ and $\mathbf{f}_3(0) = \mathbf{e}_3(0)$, and we choose $k = 0$ so that

$$\mathbf{w}_0 = 1, \quad \mathbf{w}_1 = \gamma\left(\cos\psi - \mathrm{i}\,\sin\psi\right). \tag{42}$$

Example 1. For the choices $\psi = 0.6\,\pi$ and $\xi = 1$, the coefficients of the two complex polynomials (5) are

$$\boldsymbol{\alpha}_0 = 0.9704810184, \quad \boldsymbol{\alpha}_1 = 1.251475360 - 0.3265209207\,\mathrm{i},$$

$$\boldsymbol{\alpha}_2 = -1.446585247 + 0.2549451564\,\mathrm{i}, \quad \boldsymbol{\alpha}_3 = -0.2998951274 + 0.9229822965\,\mathrm{i},$$

$$\boldsymbol{\beta}_0 = \boldsymbol{\beta}_3 = 0, \quad \boldsymbol{\beta}_1 = 1.538791812, \quad \boldsymbol{\beta}_2 = 0.4755128207 - 1.463477980\,\mathrm{i},$$

and for the intermediate control points (32) we obtain

$$\mathbf{p}_1 = (\,0.1345476296, 0, 0\,), \quad \mathbf{p}_2 = (\,0.3080523555, 0.2133383207, 0\,),$$

$$\mathbf{p}_3 = (\,0.1682526896, 0.5698386792, -0.004975174708\,),$$

$$\mathbf{p}_4 = (\,-0.1734469691, 0.4215900651, 0.2609811595\,),$$

$$\mathbf{p}_5 = (\,-0.2301381628, 0.2133383207, 0\,), \quad \mathbf{p}_6 = (\,-0.1345476296, 0, 0\,).$$

The resulting curve is shown in Figure 5 together with the Frenet frame (left) and the ERF (right), which is not periodic since $\psi \neq 0$. Figure 6 shows two different periodic rational adapted frames obtained from (40)–(42) with $\gamma = -1$ (left), $\gamma = 1$ (right). The curvature and torsion profiles in Figure 7 show that the curvature is continuous but the torsion is not (see Lemma 2).

It is apparent from Figure 6 that the parameter γ exerts a strong influence on the variation of the periodic frame. The frame quality can be characterized by the *twist* [10], indicating the total rotation of the normal–plane vectors about the tangent along the curve. For the ERF (38), the twist can be expressed as

$$T_{\mathrm{ERF}} = \int_0^1 \omega_1(t)\,\sigma(t)\,\mathrm{d}t, \quad \omega_1 = 2\,\frac{uv' - u'v - pq' + p'q}{\sigma^2},$$
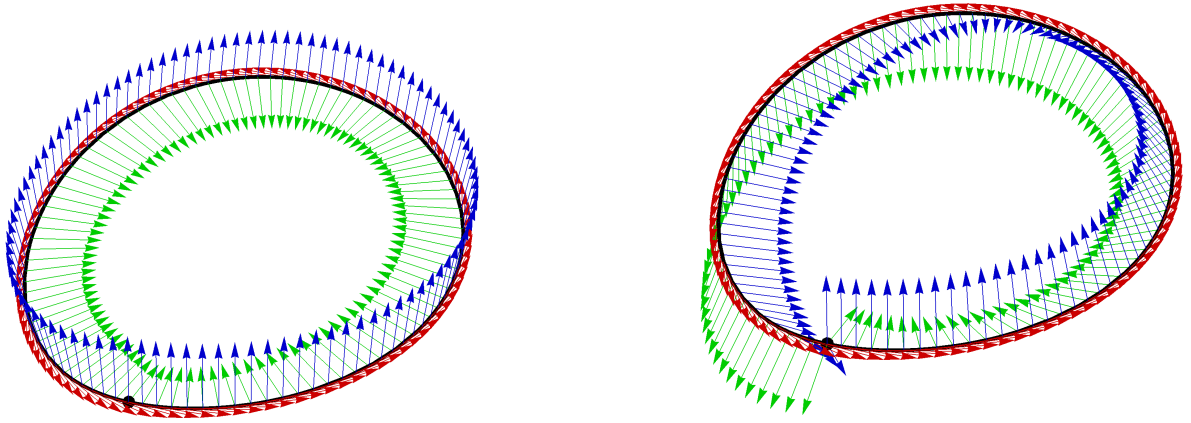
16

Figure 5: The C^2 closed–loop PH curve, constructed in Example 1, showing the Frenet frame (left) and the ER frame (right). The loop juncture point $\mathbf{r}(1) = \mathbf{r}(0)$ is indicated by a dot.
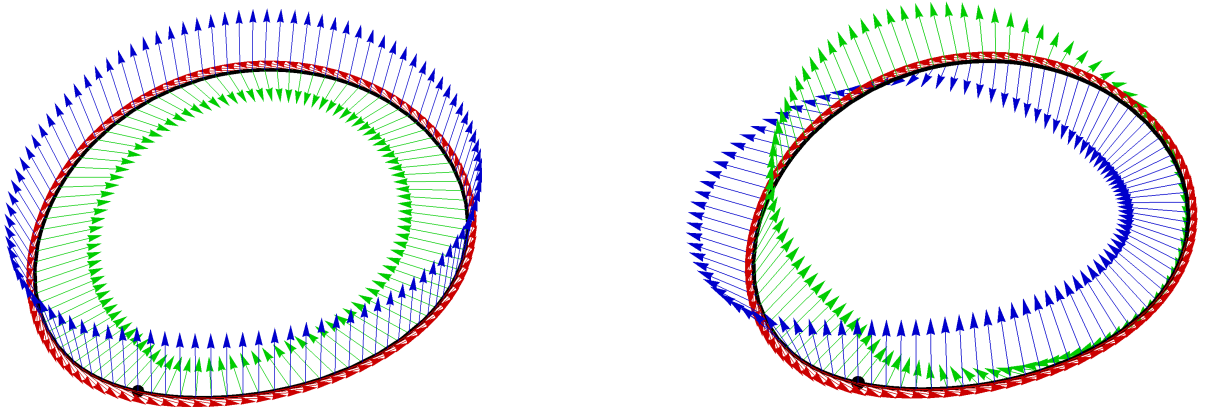

Figure 6: The C^2 closed–loop PH curve, constructed in Example 1, equipped with periodic rational adapted frames that are obtained by rotating the normal plane ER vectors, where the rotation is determined by (42) with $\gamma = -1$ (left), $\gamma = 1$ (right).
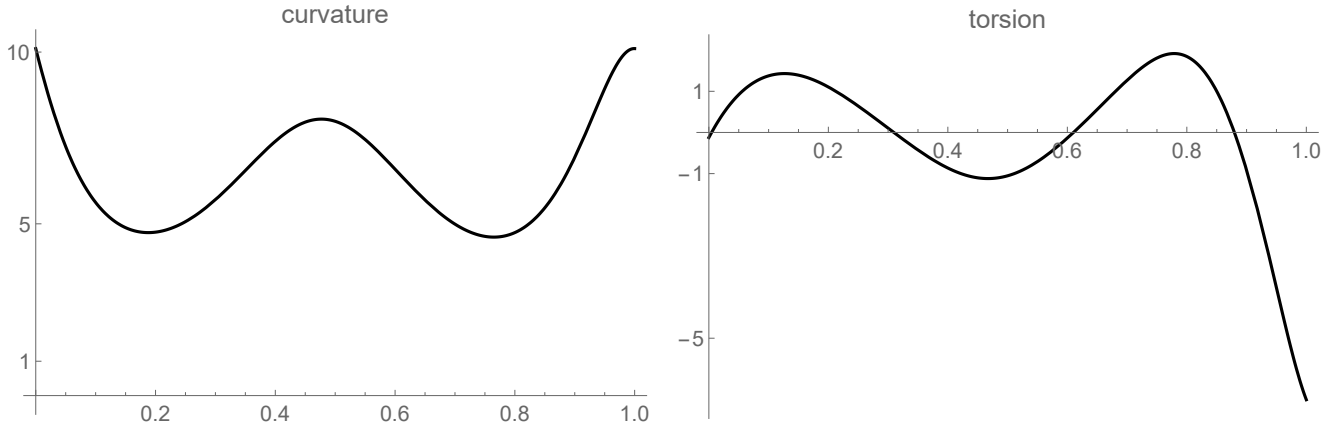
17

Figure 7: Curvature (left) and torsion (right) of the C^2 closed–loop PH curve in Example 1.

where ω_1 is the angular velocity component in the tangent direction, while for the rotated frame (40) the twist depends on γ, and is given by

$$T_\gamma = \int_0^1 \Omega_1(t)\,\sigma(t)\,\mathrm{d}t, \quad \Omega_1(t) = \omega_1(t) + \frac{\theta'(t)}{\sigma(t)}, \tag{43}$$

where

$$\theta(t) = 2\,\tan^{-1}\frac{b(t)}{a(t)} = 2\,\tan^{-1}\frac{-\gamma\,t\,\sin\psi}{1 - t + \gamma\,t\,\cos\psi}.$$

For $\psi \in (-\pi, \pi)$ we obtain, by straightforward computations,

$$T_\gamma = T_{\mathrm{ERF}} - 2\psi + \begin{cases} 0, & \gamma > 0, \\[2mm] 2\,\pi\,\mathrm{sign}(\psi), & \gamma < 0. \end{cases}$$

113 This shows that T_γ has, for any fixed ψ, a piecewise–constant dependence on γ.

However, the integral (43) is not a satisfactory indicator of the frame quality if the integrand changes sign on the integration interval (i.e., a cancellation of "positive" and "negative" twist occurs). To address this, one can consider the *absolute twist* defined by

$$T_{\mathrm{abs},\gamma} := \int_0^1 |\Omega_1(t)|\,\sigma(t)\,\mathrm{d}t.$$

114 To evaluate this quantity, the *inflections* of the adapted frame $(\mathbf{f}_1, \mathbf{f}_2, \mathbf{f}_3)$ — i.e., the points on $(0,1)$ where $\Omega_1(t)$
115 changes sign — must be identified.

116 **Example 2.** Choosing $\psi = 0.6\,\pi$ and $\xi = 1$, as in Example 1, the integrand Ω_1 is of constant sign on $[\,0,1\,]$ for all
117 $\gamma > 0$, but changes sign on $[\,0,1\,]$ if $\gamma < 0$. The graph of $T_{\mathrm{abs},\gamma}$ is shown in Figure 8 (left), from which we see that
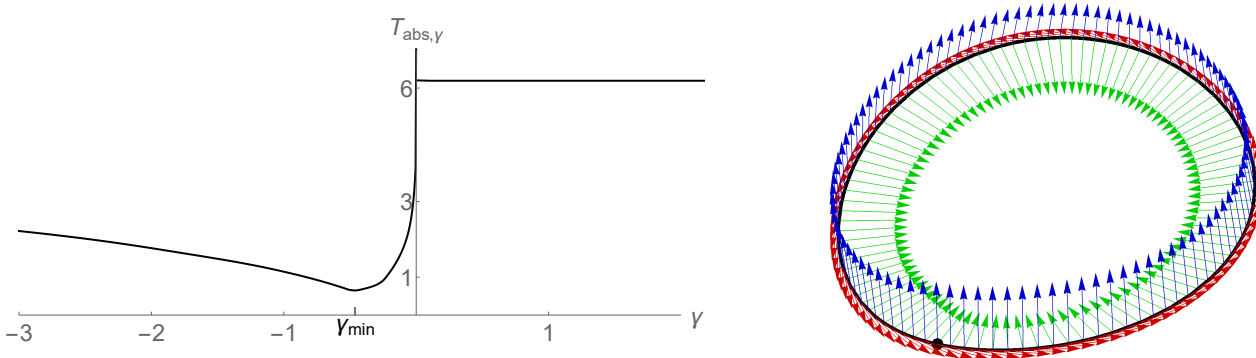
18

Figure 8: Left: Graph of $T_{\mathrm{abs},\gamma}$ in dependence of γ for $\psi = 0.6\pi$ and $\xi = 1$. Right: Periodic rational adapted frame for $\gamma = -0.46209$.

the absolute twist is much smaller for negative γ (away from zero). This explains the difference between the frames in Figure 6, since $T_{\mathrm{abs},-1} = 1.14628 \ll T_{\mathrm{abs},1} = 6.19326$. The minimum of $T_{\mathrm{abs},\gamma}$ is attained for $\gamma_{\min} = -0.46209$, $T_{\mathrm{abs},\gamma_{\min}} = 0.65175$, and the corresponding frame is shown in Figure 8 (right).

Further details on optimization of the twist for minimal twist frames on open curves, and periodic frames on closed–loop curves, may be found in [9, 10].

The periodic rational adapted frames defined by (40)–(42) are, in general, only C^0 continuous. However, by an appropriate choice of the parameter γ, one can also achieve C^1 continuity. Imposing the additional condition $\Omega_1(0) = \Omega_1(1)$ for C^1 continuity results in the quadratic equation $\gamma^2 \sin\psi - 3\gamma\xi - \sin\psi = 0$ in γ, with the two solutions

$$\gamma_\pm := \frac{3\xi \pm \sqrt{9\xi^2 + 4\sin^2\psi}}{2\sin\psi}.$$

It can be verified that, with these two γ values, we have $\mathbf{f}_i'(1) = \mathbf{f}_i'(0)$, $i = 1, 2, 3$ — i.e., the frame vectors are C^1 continuous at the juncture point. This property is particularly useful in the construction of swept surfaces of the form

$$\mathbf{S}(t, u) = \mathbf{r}(t) + p_1(u)\,\mathbf{f}_2(t) + p_2(u)\,\mathbf{f}_3(t),$$

where $\mathbf{p}(u) = (p_1(u), p_2(u))$ is a given planar curve.

Example 3. For the choice $\psi = 0.6\pi$ and $\xi = 1$, we have $\gamma_- = -0.290302$, $T_{\mathrm{abs},\gamma_-} = 0.816884$ and $\gamma_+ = 3.44469$, $T_{\mathrm{abs},\gamma_+} = 6.19326$. Figure 9 shows a swept surface with $\mathbf{r}(t)$ from Example 1, the frame computed using γ_-, and $\mathbf{p}(u)$ chosen as the planar closed–loop PH curve from Section 4.3 (with $\psi = 0.5\pi$, $\xi = 0$, and arc length $S = 0.5$).
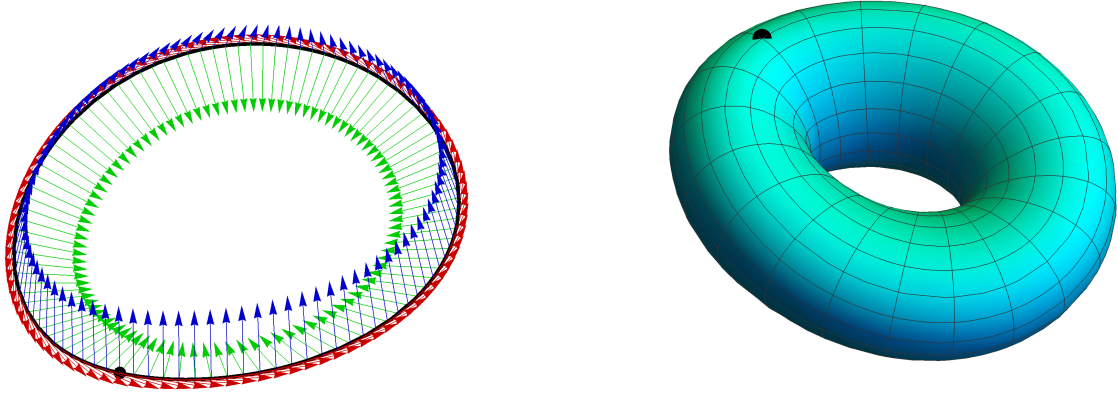
19

Figure 9: Left: the C^1 periodic rational adapted frame for $\gamma = \gamma_-$ (see Example 3). Right: the corresponding swept surface $\mathbf{S}(t, u)$.

Example 4. With $\psi = 0.1\,\pi$ and $\xi = -1$, the minimum value of the absolute twist is obtained for any $\gamma > 0$, namely $T_{\mathrm{abs},\gamma} = 2.61674$ — see Figure 10. The frame is C^1 continuous for $\gamma_- = -9.81014$ with $T_{\mathrm{abs},\gamma_-} = 5.36089$, and $\gamma_+ = 0.101935$ with $T_{\mathrm{abs},\gamma_+} = 2.61674$. The corresponding swept surface for γ_+ with $\mathbf{p}(u)$ determined by $\psi = 0.5\,\pi$, $\xi = 0$ and arc length $S = 0.2$ is shown in Figure 10 (right).

Remark 3. The ERF is useful in constructing a rational *rotation–minimizing frame* (RMF) or *minimal twist frame* (MTF) on spatial PH curves — see [2, 5, 6, 9, 10, 11]. For a certain family of degree 7 PH curves, the ERF is itself an RMF [2] — these curves are characterized [8] by the constraints

$$\mathrm{Im}(\overline{\boldsymbol{\alpha}}_0\boldsymbol{\alpha}_1 + \overline{\boldsymbol{\beta}}_0\boldsymbol{\beta}_1) \;=\; \mathrm{Im}(\overline{\boldsymbol{\alpha}}_0\boldsymbol{\alpha}_2 + \overline{\boldsymbol{\beta}}_0\boldsymbol{\beta}_2) \;=\; 0\,,$$

$$3\,\mathrm{Im}(\overline{\boldsymbol{\alpha}}_1\boldsymbol{\alpha}_2 + \overline{\boldsymbol{\beta}}_1\boldsymbol{\beta}_2) + \mathrm{Im}(\overline{\boldsymbol{\alpha}}_0\boldsymbol{\alpha}_3 + \overline{\boldsymbol{\beta}}_0\boldsymbol{\beta}_3) \;=\; 0\,,$$

$$\mathrm{Im}(\overline{\boldsymbol{\alpha}}_1\boldsymbol{\alpha}_3 + \overline{\boldsymbol{\beta}}_1\boldsymbol{\beta}_3) \;=\; \mathrm{Im}(\overline{\boldsymbol{\alpha}}_2\boldsymbol{\alpha}_3 + \overline{\boldsymbol{\beta}}_2\boldsymbol{\beta}_3) \;=\; 0\,,$$

on the coefficients of the polynomials (5). For the C^2 closed–loop PH curves of degree 7 considered herein, these conditions cannot be satisfied, since the number of constraints exceeds the number of free parameters. Moreover, when we relax the smoothness conditions and consider C^1 closed–loop PH curves, only trivial (planar) cases are compatible with the above constraints. This can be verified as follows. Using the coefficients (13) for a C^1 closed
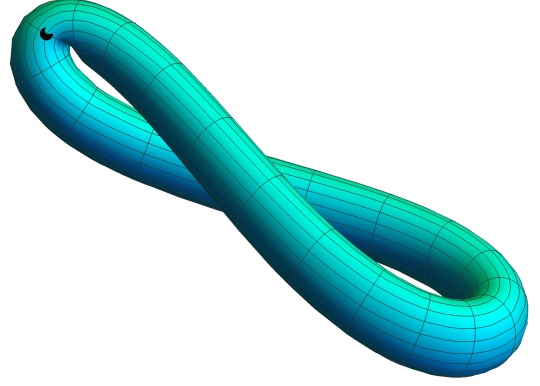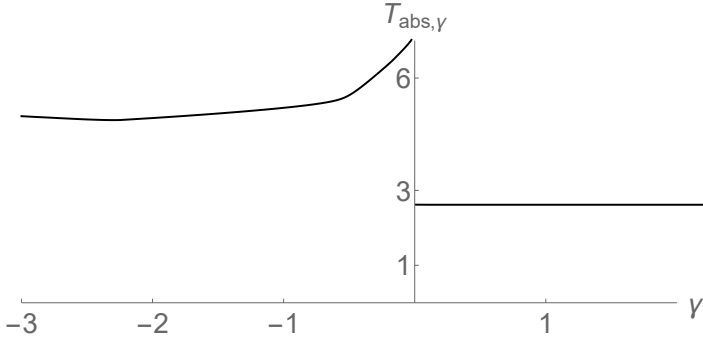
20

Figure 10: Left: Graph of $T_{\mathrm{abs},\gamma}$ in dependence of γ for $\psi = \pi/10$ and $\xi = -1$. Right: Swept surface obtained with the C^1 periodic rational adapted frame for $\gamma = \gamma_+$ (see Example 4).

loop, and writing $\boldsymbol{\alpha}_1 = w\,a_1\mathrm{e}^{\mathrm{i}\,\psi_1}$, $\boldsymbol{\alpha}_2 = w\,a_2\mathrm{e}^{\mathrm{i}\,\psi_2}$ and $\boldsymbol{\beta}_1 = w\,b_1\mathrm{e}^{\mathrm{i}\,\phi_1}$, $\boldsymbol{\beta}_2 = w\,b_2\mathrm{e}^{\mathrm{i}\,\phi_2}$ with $w \neq 0$, the constraints reduce to

$$a_1 \sin(\psi_1 - \psi_0) \;=\; a_2 \sin(\psi_2 - \psi_0) \;=\; 0\,,$$

$$3\,[\,a_1 a_2 \sin(\psi_2 - \psi_1) + b_1 b_2 \sin(\phi_2 - \phi_1)\,] \;+\; \sin(\psi_3 - \psi_0) \;=\; 0\,,$$

$$a_1 \sin(\psi_3 - \psi_1) \;=\; a_2 \sin(\psi_3 - \psi_2) \;=\; 0\,.$$

Any values $a_1, a_2, b_1, b_2, \psi_0, \psi_1, \psi_2, \psi_3, \phi_1, \phi_2$ satisfying these conditions yield $\boldsymbol{\alpha}(t) = \mathrm{e}^{\mathrm{i}\,\zeta}\,a(t)$, $\boldsymbol{\beta}(t) = \mathrm{e}^{\mathrm{i}\,\eta}\,b(t)$ for real polynomials $a(t), b(t)$ so $\mathbf{r}'(t)$ has the components $x'(t) = a^2(t) - b^2(t)$, $y'(t) = 2\,\cos(\zeta - \eta)\,a(t)b(t)$, $z'(t) = 2\,\sin(\zeta - \eta)\,a(t)b(t)$. Hence, $\mathbf{n} \cdot \mathbf{r}'(t) \equiv 0$ for $\mathbf{n} = (0, \sin(\zeta - \eta), -\cos(\zeta - \eta))$, and consequently $\mathbf{r}(t)$ degenerates to a plane curve.

Finally, we consider employing the C^2 closed–loop PH curves $\mathbf{r}(t)$, $t \in [0, 1]$ for the construction of *tubular surfaces*. Namely, choosing a trajectory $\mathbf{c}(u)$ for the juncture point, a rotation matrix $R(u)$, and a scaling function $\rho(u)$ for $u \in I \subset \mathbb{R}$, we define a surface

$$\mathbf{S}(t, u) \;=\; \rho(u)\,\mathbf{r}(t)\,R(u)^T + \mathbf{c}(u), \quad (t, u) \in [0, 1] \times I,$$

whose isoparametric curves $u = u_0 =$ constant are C^2 closed–loop PH curves with arc length $\rho(u_0)$. If $\mathbf{c}(u)$, $R(u)$,

21

and $\rho(u)$ depend rationally on u, then $\mathbf{S}(t,u)$ is a rational surface. Note that a rational rotation matrix can be obtained from (38) by any choice of polynomials u,v,p,q using $\mathbf{e}_i$, $i = 1,2,3$ as the columns of R. An example of these tubular surfaces is shown in Figure 11.
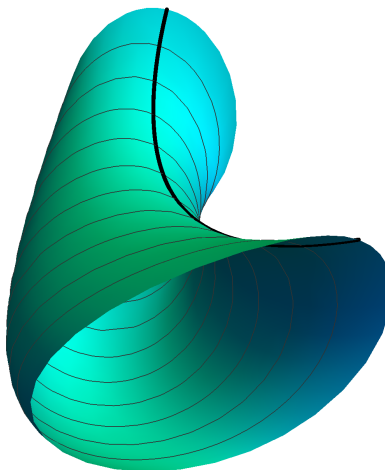

Figure 11: An example tubular surface constructed by translating, rotating, and scaling the C^2 closed–loop PH curve curve from Example 1.

6. Closure

The existence of a two–parameter family of non–planar C^2 closed loops with specified arc lengths, defined by degree 7 Pythagorean–hodograph (PH) space curves, has been demonstrated. Using the Hopf map representation for a PH space curve $\mathbf{r}(t)$, $t \in [0,1]$, and adopting a canonical coordinate system with the juncture point $\mathbf{r}(1) = \mathbf{r}(0)$ at the origin and tangent in the positive x–direction, and a total arc length $S = 1$, these C^2 closed–loop curves admit a closed–form construction procedure that employs only elementary arithmetic operations and a few (real) square-root extractions.

Explicit formulae for the Bézier control points of the closed–loop curves were derived, exhibiting their dependence on the two free parameters, and the values of these parameters that incur certain symmetry properties, or degeneration to planar curves, were identified. The construction of rational adapted orthonormal frames with C^0 or C^1 continuity at the loop juncture point was also addressed, and these frames were employed to formulate families of rational swept surfaces. Finally, a family of tubular surfaces defined by translation, rotation, and scaling of the degree 7 C^2 closed–loop PH curves was demonstrated.

The focus of the present study has been to demonstrate the feasibility of closed–form solutions for the construction of C^2 closed–loop PH curves with specified arc lengths, and to elucidate their key properties and special cases. To facilitate their use in design contexts, further investigation is required on how to exploit the two free parameters for shape optimization, or to satisfy additional desired geometrical constraints. The exploitation of the C^2 closed–loop curves in specific applications, such as motion control in robotics, manufacturing, or automated inspection, also deserves further investigation.

References

[1] H. L. Bray and J. L. Jauregui (2015), On curves with nonnegative torsion, *Archiv der Mathematik* **104**, 561–575.

[2] H. I. Choi and C. Y. Han (2002), Euler–Rodrigues frames on spatial Pythagorean–hodograph curves, *Comput. Aided Geom. Design* **19**, 603–620.

[3] H. I. Choi, D. S. Lee, and H. P. Moon (2002), Clifford algebra, spin representation, and rational parameterization of curves and surfaces, *Adv. Comp. Math.* **17**, 5–48.

[4] R. T. Farouki (2008), *Pythagorean–Hodograph Curves: Algebra and Geometry Inseparable*, Springer, Berlin.

[5] R. T. Farouki (2010), Quaternion and Hopf map characterizations for the existence of rational rotation–minimizing frames on quintic space curves, *Adv. Comp. Math.* **33**, 331–348.

[6] R. T. Farouki, C. Giannelli, C. Manni, and A. Sestini (2012), Design of rational rotation–minimizing rigid body motions by Hermite interpolation, *Math. Comp.* **81**, 879–903.

[7] R. T. Farouki, C. Giannelli, and A. Sestini (2019), Rational minimal–twist motions on curves with rotation–minimizing Euler–Rodrigues frames, *J. Comput. Appl. Math.* **352**, 240–254.

181 [8] R. T. Farouki, C. Y. Han, P. Dospra, and T. Sakkalis (2013), Rotation–minimizing Euler–Rodrigues

182 rigid–body motion interpolants, *Comput. Aided Geom. Design* **30**, 653–671.

183 [9] R. T. Farouki, S. H. Kim, and H. P. Moon (2019), Rational adapted orthonormal frames of minimal twist

184 along closed space curves, preprint.

185 [10] R. T. Farouki and H. P. Moon (2018), Rational frames of minimal twist along space curves under specified

186 boundary conditions, *Adv. Comp. Math.* **44**, 1627–1650.

187 [11] C. Y. Han (2008), Nonexistence of rational rotation–minimizing frames on cubic curves, *Comput. Aided Geom.*

188 *Design* **25**, 298–304.

189 [12] D. Hilbert and S. Cohn–Vossen (1952), *Geometry and the Imagination* (translated by P. Nemenyi), Cheslea

190 Publishing Company, New York, reprint.

191 [13] E. Kreyszig (1959), *Differential Geometry*, University of Toronto Press.

192 [14] R. S. Millman and G. D. Parker (1977), *Elements of Differential Geometry*, Prentice–Hall, Englewood Cliffs,

193 NJ.

194 [15] C. C. Pansonato and S. I. R. Costa (2008), Total torsion of curves in three–dimensional manifolds, *Geom.*

195 *Dedicata* **136**, 111–121.

24